Proliferative advantage of specific aneuploid cells drives evolution of tumor karyotypes

Ivana Ban[1*], Lucija Tomašić[1*], Marianna Trakala[2], Iva M. Tolić[3], Nenad Pavin[1#]

[1]Department of Physics, Faculty of Science, University of Zagreb, Bijenička cesta 32, 10000 Zagreb, Croatia
[2]David H. Koch Institute for Integrative Cancer Research, Howard Hughes Medical Institute, Massachusetts Institute of Technology, Cambridge, Massachusetts 02142, USA;
[3]Division of Molecular Biology, Ruđer Bošković Institute, Bijenička cesta 54, 10000 Zagreb, Croatia

[*]These authors contributed equally to this work.
[#]Correspondence: npavin@phy.hr (N.P.)

ABSTRACT

Most tumors have abnormal karyotypes, which arise from mistakes during mitotic division of healthy euploid cells and evolve through numerous complex mechanisms. In a recent mouse model with high levels of chromosome missegregation, chromosome gains dominate over losses both in pretumor and tumor tissues, whereas tumors are characterized by gains of chromosomes 14 and 15. However, the mechanisms driving clonal selection leading to tumor karyotype evolution remain unclear. Here we show, by introducing a mathematical model based on a concept of a macro-karyotype, that tumor karyotypes can be explained by proliferation-driven evolution of aneuploid cells. In pretumor cells, increased apoptosis and slower proliferation of cells with monosomies lead to predominant chromosome gains over losses. Tumor karyotypes with gain of one chromosome can be explained by karyotype-dependent proliferation, while for those with two chromosomes an interplay with karyotype-dependent apoptosis is an additional possible pathway. Thus, evolution of tumor-specific karyotypes requires proliferative advantage of specific aneuploid karyotypes.

Keywords: karyotype evolution, tumor karyotype, aneuploidy, mathematical model, theory, cell proliferation, apoptosis, chromosome missegregation, macro-karyotype

INTRODUCTION

During cell division, missegregation of duplicated chromosomes generates cells with perturbed karyotypes, a condition with abnormal chromosome number known as aneuploidy. Aneuploidy has detrimental effect on cell vitality and proliferation, and is linked with cancer and other diseases (Ben-David & Amon, 2019; Gordon et al., 2012; Hwang et al., 2021; Weaver & Cleveland, 2006). While in healthy cells, aneuploidy causes a strong anti-proliferative response as a result of gene dosage imbalances (Santaguida et al., 2015) this response can be overcome in cancer cells, allowing the increased frequency of errors to promote aneuploid karyotype evolution and acceleration of tumor formation (Duijf & Benezra, 2013; van Jaarsveld & Kops, 2016). These ideas have emerged from extensive studies of aneuploidy in different systems including cell lines (Cimini et al., 2001; Thompson & Compton, 2008, 2011a), organoids (Bolhaqueiro et al., 2019; Drost & Clevers, 2018; Narkar et al., 2021), animal models (Bolton et al., 2016; Sheppard et al., 2012; Shoshani et al., 2021; Trakala et al., 2021), as well as theoretically (Araujo et al., 2013; Desper et al., 2005; Elizalde et al., 2018; Gusev et al., 2000, 2001; Laughney et al., 2015; Lynch et al., 2021). Yet, how the interplay between chromosome missegregation, cell proliferation and other processes drives long-term karyotype evolution is poorly understood.

One of key processes which drives karyotype evolution is chromosome missegregation, which is increased for many tumor karyotypes and termed chromosome instability (CIN) (Hintzen et al., 2021; Nicholson & Cimini, 2013; Thompson & Compton, 2008). Missegregation includes gain or loss of one or a few chromosomes due to incorrect attachment of chromosomes to the mitotic spindle (Bakhoum et al., 2009; Cimini, 2008; Dewhurst et al., 2014; Nicholson et al., 2015; Thompson & Compton, 2011b). Another key process for karyotype evolution is cell proliferation, which determines how the total number of cells with a certain karyotype changes over time. In particular, it was measured that aneuploid cells typically proliferate slower than euploid cells (Hintzen et al., 2021; Williams et al., 2008). However, certain aneuploid karyotypes with a favorable combination of chromosome gains or losses can lead to enhanced cell proliferation (Ben-David et al., 2014; Heyde et al., 2021; Rohban & Campaner, 2015). In contrast, other aneuploid karyotypes can result in malfunctional cell physiology and consequently apoptosis.

Studying how different processes affect long-term karyotype evolution is experimentally challenging because it requires tracking of all relevant karyotypes over many generations. An alternative approach is mathematical modeling in which simple hypotheses can be explored beyond experimental constraints. Modeling is powerful because it allows to identify the dominant mechanisms in the existing experiments and provides ideas for new experiments targeted on testing specific model predictions. Theoretical models of karyotype evolution have been designed to study certain key aspects of this complex process. Early theoretical studies investigated the role of chromosome missegregation on karyotype evolution, leading to a theoretical upper limit for the missegregation rate that allows diploid cells to survive (Gusev et al., 2000, 2001). To study how karyotype evolution depends on genetic linkage, genes controlling cell proliferation, apoptosis and chromosome missegregation were placed on two chromosomes in different combinations (Araujo et al., 2013). A study of karyotype evolution that includes the interplay between missegregation and whole genome duplication found that population converges to near triploid state (Laughney et al., 2015), and that heterogeneity is primary influenced by the missegregation rate (Elizalde et al., 2018). Recently, a theoretical model was developed to measure CIN from karyotype diversity within a tumor (Lynch et al., 2021).

Development of novel mouse models with high levels of chromosome missegregation enabled experimental exploration of karyotype evolution during tumor initiation and growth

(Trakala et al., 2021,Shoshani et al., 2021). Quantification of chromosomal gains and losses in these mouse models revealed that chromosome gains dominate over losses both in pretumor and tumor tissues. At early stages of T-cell development in the thymus, 90% of cells are euploid due to strong selection, whereas in later stages cells accumulate more errors and a larger fraction, up to 60-80% of cells become aneuploid, where individual chromosomes are roughly equally gained, on average 4% over aneuploid cells (Trakala et al., 2021). In contrast, when T-cell lymphomas start to develop, there is a dramatic increase in gains of chromosomes 14 and 15 in almost 100% of aneuploid cells, whereas the average gain of other chromosomes remains around 8%. These results suggested that lymphomas developed through clonal selection of favorable aneuploidies. However, the mechanisms of clonal selection leading to tumor karyotype evolution from euploid karyotypes remain unclear.

In this paper we explore the idea that karyotype-dependent proliferation and apoptosis are key drivers of clonal selection that leads to aneuploidy observed in tumor cells. To describe a large number of karyotype combinations that arise due to missegregation, we introduce a "macro-karyotype model" in which we follow the copy number of specific chromosomes, together with the total number of gains and losses for other chromosomes. By solving the model we find that only a small fraction of chromosome missegregation events generates tumor-specific karyotypes, but thanks to their proliferative advantage, cells with these karyotypes eventually overtake the population in agreement with the experimentally observed karyotype evolution. Thus, the central finding of our theory is that, under conditions of high chromosome missegregation, tumor-specific karyotypes arise from proliferative advantage of specific aneuploid karyotypes.

RESULTS

Mathematical model for tumor karyotype evolution

Theoretical exploration of tumor karyotype evolution poses two main challenges: tumor tissues consist of a large number of karyotype combinations and a large number of cells. To tackle these problems, we design a novel approach based on a concept of a macro-karyotype. We define a macro-karyotype as a karyotype that contains the copy number of specific chromosomes that are crucial for the process of interest, whereas for other chromosomes only the total chromosome gains and losses are counted. Macro-karyotypes contain all relevant information about the exact cell karyotype, while substantially reducing the number of karyotype combinations and allowing for the use of mean-field calculations, which can describe large populations. Thus, the strength of this approach lies in that it allows us to follow karyotype evolution for a virtually unlimited number of cells and generations.

In our macro-karyotype model we calculate karyotype evolution and a corresponding pedigree tree (**Fig. 1a**). Karyotype of a cell with n different chromosomes is described by a vector, $\mathbf{K} \equiv (c_1, \dots, c_n)$, in which c_i denotes copy number of i-th chromosome (**Fig. 1b**). Because some karyotypes are frequently used, we introduce a notation for them. First, diploid karyotype is denoted as a vector $\mathbf{K}_{2n} \equiv (c_1 = 2, \dots, c_n = 2)$. Second, karyotypes with at least one chromosome loss form a set of karyotypes $K_- = \{(c_1, \dots, c_n) | \exists\, c_i = 1,\ i = 1, \dots, n\}$, whereas karyotypes with chromosome gains form a set $K_+ = \{(c_1, \dots, c_n) | \exists\, c_i \geq 3,\ i = 1, \dots, n\}$. Finally, we introduce a notation for a set of karyotypes with gain of chromosome 15, $K_{+15} = \{(c_1, \dots, c_n) |\ c_{15} \geq 3\}$, and a set of karyotypes with gain of chromosomes 14 and 15, $K_{+14,+15} = \{(c_1, \dots, c_n) |\ c_{14} \geq 3, c_{15} \geq 3\}$. Note that karyotypes with chromosome losses and gains belong to more than one set.

By constructing a pedigree tree, we follow multiple generations of cells, starting from a founder cell in generation $g = 0$ (**Fig. 1a**). In generation g the number of cells (branches) can be up to 2^g, where each cell (branch) has a unique index $j = 0, \dots, 2^g - 1$. Because some branches of the pedigree tree are pruned when a cell undergoes apoptosis, cells with corresponding index j are missing and the total number of cells in that generation is smaller than 2^g.

Cell lifetime, t_0, depends on the karyotype and ends with either division or apoptosis, which occur with probabilities $1 - p_a$ and p_a, respectively (**Fig. 1c**). During cell division chromosomes can divide correctly, where each half of the duplicated chromosome (chromatid) goes to one of the two daughter cells, or missegregate, where both chromatids end up in the same cell. These events depend on the karyotype and occur with probabilities p_d and p_m, respectively (**Fig. 1c**). In our model, chromosome missegregation events are independent and the missegregation probability per cell is calculated as $p_m = \sum_{i=1}^{n} p_{m_i}$. This approximative expression holds for rare events, $p_m \ll 1$. Missegregation probability of the i-th chromosome, p_{m_i}, is calculated as the copy number of that chromosome multiplied by its probability to missegregate, p_0, $p_{m_i} = p_0 c_i$. These probabilities, together with cell lifetime and their positions in a pedigree tree, define a discrete stochastic model for karyotype evolution.

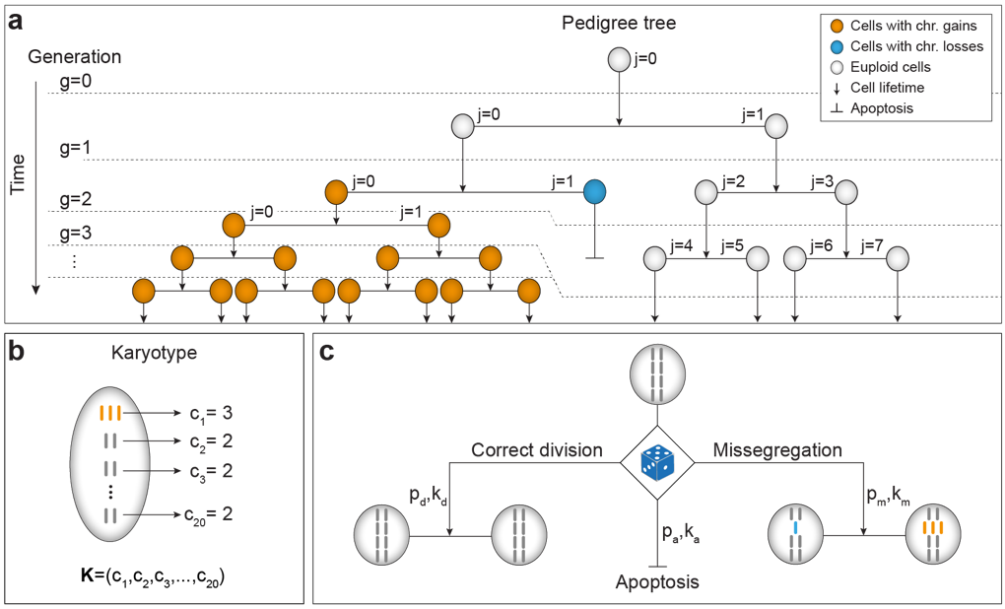

Figure 1. Mathematical model for tumor karyotype evolution. a, Scheme of the pedigree tree. Mother cell (gray circle) in generation $g = 0$ and with cell index $j = 0$ divides faithfully to two daughter cells (gray circles) with cell indexes $j = 0$ and $j = 1$ in generation $g = 1$. A chromosome missegregation event occurred yielding one daughter cell with trisomy (orange, $j = 0$) and the other with monosomy (blue, $j = 1$) at generation $g = 2$. Cells with trisomy of specific chromosome divide faster which is represented by a shorter arrow. Cells can also undergo apoptosis ($g = 2$, $j = 1$). Generations are visually divided by horizontal dashed lines which can be cascading due to different proliferation rates for diploid and aneuploid cells. **b**, Mathematical description of cell karyotype. Cell (gray oval) contains n chromosomes (rods). First chromosome has 3 copies (orange rods, $c_1 = 3$), and the other chromosomes have 2 copies (gray rods, $c_2 = c_3 = \dots = c_n = 2$). Karyotype of a cell is fully described by $c_1, \dots, c_n$. **c**, Processes included in our model. Mother cell probabilistically (dice) undergoes one of 3 processes: correct division, missegregation or apoptosis, with respective probabilities p_d, p_m, p_a and respective rates k_d, k_m, k_a. Only 4 chromosomes depicted.

Rate equation for population of cells

While the stochastic model can follow each individual cell, the main disadvantage is that it cannot follow all cells for a large number of generations. To circumvent this issue, we develop a mean-field approach, which allows us to start with a large number of cells and follow them over many generations. Here, we first calculate the probability for finding a cell with a given karyotype at the position within the pedigree tree, $P_{g,j}(\mathbf{K})$, by taking into account that cells in the generation g appear by division of the cells in the previous generation, $g-1$, whereas the cells in the generation g disappear upon cell division or apoptosis. To calculate how these probabilities evolve in time, t, we introduce the following equation:

$$\begin{aligned}\frac{dP_{g,j}(\mathbf{K})}{dt} &= k_{\mathrm{d}}(\mathbf{K})P_{g-1,\lfloor\frac{j}{2}\rfloor}(\mathbf{K}) + \frac{1}{2}\sum_{i=1}^{n} k_{\mathrm{m}_i}(\mathbf{K}+\mathbf{e}_i)P_{g-1,\lfloor\frac{j}{2}\rfloor}(\mathbf{K}+\mathbf{e}_i) \\ &+ \frac{1}{2}\sum_{i=1}^{n} k_{\mathrm{m}_i}(\mathbf{K}-\mathbf{e}_i)P_{g-1,\lfloor\frac{j}{2}\rfloor}(\mathbf{K}-\mathbf{e}_i) - [k_{\mathrm{d}}(\mathbf{K}) + k_{\mathrm{m}}(\mathbf{K}) + k_{\mathrm{a}}(\mathbf{K})]P_{g,j}(\mathbf{K})\,.\end{aligned} \tag{1}$$

Here, the first term on the right-hand side describes how a cell with karyotype $\mathbf{K}$ in generation $g-1$, which we refer to as the mother cell, correctly divides into two cells of the same karyotype in generation g, which we refer to as daughter cells. The second and third terms describe missegregation in which the mother cells with karyotypes $\mathbf{K}\pm\mathbf{e}_i$ lose or gain the ith chromosome, yielding one daughter cell with karyotype $\mathbf{K}$. The last term describes division or apoptosis of the daughter cell and therefore appears with a negative sign. The unit vector $\mathbf{e}_i$ has the value 1 in the ith coordinate and 0's elsewhere.

Indices in Eq. (1) describe the position in the pedigree tree, where each daughter which belongs to generation g and branch j, originates from a mother cell in generation $g-1$ with the corresponding branch $\lfloor j/2\rfloor$ (**Fig. 1a**). The floor function $\lfloor\ \ \rfloor$ ensures that two daughter cells correspond to one mother cell, one daughter cell with even and the other with odd index j. In the case of missegregation, each daughter cell has the same probability to acquire one chromosome extra or less. However, only the daughter cell with karyotype $\mathbf{K}$ will contribute to Eq. (1) and therefore we multiply these terms by 1/2.

The rates in Eq. (1) describe correct cell division, $k_{\mathrm{d}}(\mathbf{K})$, apoptosis, $k_{\mathrm{a}}(\mathbf{K})$, and chromosome missegregation, $k_{\mathrm{m}}(\mathbf{K}) = \sum_{i=1}^{n} k_{\mathrm{m}_i}(\mathbf{K})$, where $k_{\mathrm{m}_i}(\mathbf{K})$ denotes the missegregation rate of the ith chromosome (**Fig. 1c**). The rates of apoptosis and missegregation of the ith chromosome are calculated as $k_{\mathrm{a,m}_i} = \beta p_{\mathrm{a,m}_i}/\ln 4$, where the proliferation rate relates to the lifetime of a cell as $\beta = \ln 2/t_0$. The corrective factor $\ln 4$ appears because cell division in Eq. (1) is considered as a Poisson process, where every cell divides with equal probability independent of its age, whereas in more realistic case all cells live equally long (see Supplementary note). The rate of correct division is implicitly given by $\beta = k_{\mathrm{d}} + k_{\mathrm{m}} + k_{\mathrm{a}}$.

To understand karyotype evolution it is important to calculate the number of cells of a certain karyotype in the population over time, irrespective of the position in the pedigree tree. Thus, we define this number as $N(\mathbf{K}) \equiv \sum_{g=0}^{\infty}\sum_{j=0}^{2^g-1} P_{g,j}(\mathbf{K})$ and calculate how it changes in time by summing Eq. (1) over indices g and j (see Supplementary note),

$$\begin{aligned}\frac{dN(\mathbf{K})}{dt} &= [k_{\mathrm{d}}(\mathbf{K}) - k_{\mathrm{m}}(\mathbf{K}) - k_{\mathrm{a}}(\mathbf{K})]N(\mathbf{K}) + \sum_{i=1}^{n} k_{\mathrm{m}_i}(\mathbf{K}+\mathbf{e}_i)N(\mathbf{K}+\mathbf{e}_i) \\ &+ \sum_{i=1}^{n} k_{\mathrm{m}_i}(\mathbf{K}-\mathbf{e}_i)N(\mathbf{K}-\mathbf{e}_i).\end{aligned} \tag{2}$$

The dimensionality of this rate equation is $2^{g+1}-1$ times lower than that of Eq. (1), yet it retains the complete information about the karyotypes in a cell population.

Despite the reduced dimensionality, Eq. (2) cannot be directly integrated on a supercomputer because of a huge number of karyotype combinations. For this reason, we solve Eq. (2) by reducing the space of vector $\mathbf{K}$ while retaining all the important information about the karyotype, e.g., whether it is euploid or aneuploid, whether aneuploid karyotypes contain monosomies and trisomies. Thus, we construct a vector that contains the information about the karyotype, $\mathbf{M}(\mathbf{K}) \equiv (x_1, \dots, x_L)$, which we term macro-karyotype. Here, component $x_l(\mathbf{K}) \equiv \sum_{i=1}^{n} \delta_{l,c_i}$ denotes the number of chromosomes with l copies, and index L denotes the maximal copy number of each chromosome. Because nullisomies are not described in our model, the number of different chromosomes per cell is conserved, $x_1 + \cdots + x_L = n$. Thus, the macro-karyotype defined in this manner includes multiple karyotypes. A certain macro-karyotype is obtained as a set of permutations of vector components for each chromosome c_i and the number of cells with this macro-karyotype is $\widetilde{N}(\mathbf{M}) = (x_1! \cdots x_L!)^{-1} \times \sum_{\text{all perm.}} N(\mathbf{K})$. Note that the normalization is correction for counting the same karyotype multiple times.

In order to calculate how the number of cells with a certain macro-karyotype changes in time, we sum Eq. (2) over all permutations reaching the final form of the rate equation for macro-karyotype evolution (see Supplementary note):

$$\begin{aligned}\frac{d\widetilde{N}(\mathbf{M})}{dt} = {} & \left[\tilde{k}_{\mathrm{d}}(\mathbf{M}) - \tilde{k}_{\mathrm{m}}(\mathbf{M}) - \tilde{k}_{\mathrm{a}}(\mathbf{M})\right]\widetilde{N}(\mathbf{M}) \\ & + \sum_{l=2}^{L} \tilde{k}_{\mathrm{m}_l}(\mathbf{M} - \boldsymbol{\epsilon}_{l-1} + \boldsymbol{\epsilon}_l)\widetilde{N}(\mathbf{M} - \boldsymbol{\epsilon}_{l-1} + \boldsymbol{\epsilon}_l) \\ & + \sum_{l=1}^{L-1} \tilde{k}_{\mathrm{m}_l}(\mathbf{M} + \boldsymbol{\epsilon}_l - \boldsymbol{\epsilon}_{l+1})\widetilde{N}(\mathbf{M} + \boldsymbol{\epsilon}_l - \boldsymbol{\epsilon}_{l+1}).\end{aligned} \tag{3}$$

This rate equation is derived with the assumption that rates $k_{\mathrm{d,m,a}}(\mathbf{K})$ have the same value for all permutations of $c_1, \dots, c_n$ that belong to the same macro-karyotype $\mathbf{M}$, and thus the rates obey $\tilde{k}_{\mathrm{d,m,a}}(\mathbf{M}) = k_{\mathrm{d,m,a}}(\mathbf{K})$, except in the case where $\tilde{k}_{\mathrm{m}_l}(\mathbf{M}) = l x_l \beta p_0 / \ln 4$. The unit vectors $\boldsymbol{\epsilon}_l$, $\boldsymbol{\epsilon}_{l+1}$ and $\boldsymbol{\epsilon}_{l-1}$ have the value 1 in the lth, $l+1$ and $l-1$ coordinate, respectively, and 0's elsewhere. For studying karyotypes with a specific chromosome, we generalize our approach by constructing an extended macro-karyotype $\mathbf{M}_{\mathrm{ext}}(\mathbf{K}) \equiv (x_1, \dots, x_L, c_{15})$, where the last component, which corresponds to the specific chromosome, accounts for number of copies of chromosome 15 (see Supplementary note).

The key advantage of the macro-karyotype approach is the substantially reduced dimensionality of the vector space, in comparison with the dimensionality of the original vector space. For example, in the case of a cell with $L = 6$ and $n = 20$, the number of possible macro-karyotypes is $L(n-1)^{L-1} \approx 1.5 \cdot 10^7$, which is 8 orders of magnitude smaller than the number of possible karyotypes, $L^n \approx 3.7 \cdot 10^{15}$. Thus, Eq. (3) is a unique mathematical tool that allows us to study tumor karyotype evolution because it describes a large number of cells and karyotype combinations.

Increased apoptosis and slower proliferation of cells with monosomies lead to predominant chromosome gains over losses

In order to understand the role of apoptosis and proliferation in tumor karyotype evolution, we solve our model and compare the obtained results with the experimentally found karyotypes in pretumor and tumor cells from a mouse model (Trakala et al., 2021). First, we explore under what conditions chromosome gains dominate over losses in pretumor cells, and subsequently how tumor-specific karyotypes arise.

To explore macro-karyotype evolution starting from multiple diploid cells (**Fig. 2a**), we solve Eq. (3), for which we first have to estimate model parameters (see Table 1). For euploid cells, we use the proliferation rate value $\beta(\mathbf{K}_{2n}) = 1\ \mathrm{d}^{-1}$, based on division time for the earliest thymocyte, double negative, stages (DN1-DN4) (Petrie & Zúñiga-Pflücker, 2007). For aneuploid cells, the proliferation rate is $\beta(\mathbf{K} \neq \mathbf{K}_{2n}) = 0.8\ \mathrm{d}^{-1}$, because aneuploid cells proliferate roughly 20% slower in comparison to diploid cells (Hintzen et al., 2021; Williams et al., 2008). Given that in this mouse model (Trakala et al., 2021) all cells have the same probability of missegregating their chromosomes independent of their karyotype, we use the same missegregation rates values for all karyotypes, including both euploid and aneuploid cells. Because there is no direct measurement of the missegregation rate for this mouse model, we roughly estimate it from Eq. (2) in the regime of small chromosome gains, gain $\ll 100\%$, and small number of generations in which linear relationship holds $\mathrm{gain} = p_0 t/t_0$ (see Supplementary note). Therefore, the missegregation rate is obtained from linear fit of experimentally measured chromosome gains through DN1-DN4 stages, yielding $p_0 = 0.0017$ (**Fig. 2b, Table 1**). Since the rate of apoptosis is not measured for this mouse model, we use it as a free parameter and estimate it later by comparing results of our model with experiments.

To visualize karyotype evolution, we plot a pedigree tree for the first 5 generations obtained from one run of stochastic simulations starting with one diploid cell (**Fig. 2c**). After several generations missegregation events occur yielding daughter cells with chromosome loss and chromosome gain. Aneuploid cells need more time to divide and therefore their branches are longer in comparison to branches of euploid cells. Some cells undergo apoptosis which is visible as pruned branches in the pedigree tree.

To explore how karyotypes evolve, we solve Eq. (3) and plot chromosome gains and losses in time. We find that chromosome gains and losses closely follow each other and reach a similar asymptotic value (**Fig. 2d**). In contrast, experimental data show two times more cells with chromosome gains in comparison to cells with chromosome losses (Trakala et al., 2021). To explain these experimental results, we explore two scenarios: cells with monosomies undergo increased apoptosis (S1) or cells with monosomies proliferate slower (S2), in comparison to cells with chromosome gains. To test scenario S1, we use the probability of apoptosis for monosomies $p_{\mathrm{a}}(\mathbf{K}_{-}) = 20\%$, whereas all other cells do not undergo apoptosis. We explore the karyotypes after $t = 17$ d, because this time point corresponds to stage DN4, the last stage with no significant gain of specific chromosomes. The model predicts on average 4.2% of cells with chromosome gains and 1.8% of cells with chromosome losses (**Fig. 2e**). Similar results are obtained by analyzing karyotypes of 125 cells randomly chosen from 5 runs of stochastic simulations, which also yield the information about the variability in chromosome gains and losses (**Fig. 2e**).

By comparing our theoretical results with the experimentally measured gains and losses for thymus cells in DN4 stage (**Fig. 2f**) we find that the model quantitatively explains the both average chromosome gains and losses as well as the variability of these distributions (two sample Kolmogorov-Smirnov test, *p*-value is 0.5 for chromosome gains and losses). Because experimentally observed gains and losses can be explained with the model with increased apoptosis of cells with monosomies, we conclude that gain/loss ratio can arise because of karyotype dependent apoptosis, supporting scenario S1.

To explore scenario S2, we vary the proliferation rate for vanishing apoptosis (**Fig. 2g**, ordinate). As the proliferation rate of cells with monosomies decreases, gain/loss ratio increases

and for proliferation of 0.48 d^{-1} the model yields the experimentally observed gain/loss ratio of 2.4 (**Fig. 2g**, point S2). However, it is more likely that cells with monosomies have altered both apoptosis and proliferation. Thus, we vary both parameters simultaneously, to explore the interplay between scenarios S1 and S2. We find a smooth transition from small to large gain/loss ratio as apoptosis increases and proliferation decreases (**Fig. 2g**, arrow). The experimentally observed gain/loss ratio is obtained for combinations of apoptosis and proliferation rates where both rates either increase or decrease, to compensate the effect of each other (**Fig. 2g**, white contour). We expect that increased apoptosis and slower proliferation of cells with monosomies will reduce their fitness, which is generally considered as ability of a cell to reproduce and defined as $W(\mathbf{K}) = N(\mathbf{K})^{-1} dN(\mathbf{K})/dt$. We find cells with high fitness in the region of parameter space where chromosome gains are as frequent as losses, and cells with low fitness in the region where gains dominate over losses (compare **Figs. 2g** and **2h**). These results lead us to conclude that both increased apoptosis and slower proliferation of cells with monosomies can explain experimentally measured gain/loss ratio, and that they are interchangeable.

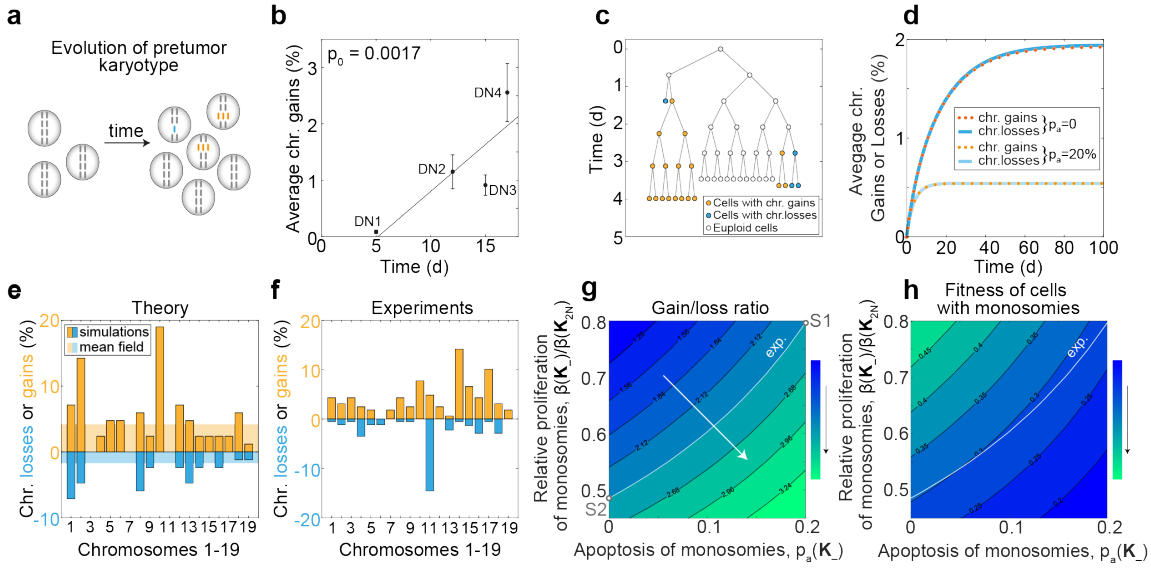

Figure 2. Increased apoptosis and decreased proliferation of cells with monosomies generate imbalance of chromosome gains and losses. a, Schematics showing cells containing one copy of chromosome (blue rod), two copies of chromosome (gray rods) and three copies of chromosome (orange rods) at two different time points. **b**, Experimentally measured average chromosome gains during T-cell lymphoma development, for stages DN1-DN4 (black circles) with duration 10 days, 4 days, 2 days, and 2 days, respectively (Porritt et al., 2003). The experimental points are positioned at the middle of duration of each phase. The line represents linear fit, gain $= p_0 t +$ offset. **c**, Pedigree tree obtained from one simulation run, showing diploid cells (white circles), cells with gains (orange circles) and losses (blue circles). **d**, Average chromosome gains (dotted orange lines) and losses (full blue lines) in time calculated by mean field approach for $p_a(\mathbf{K}) = 0$ (dark orange and dark blue) and $p_a(\mathbf{K} \neq \mathbf{K}_{2n}) = 20\%$ (light orange and light blue). **e**, Percentage of chromosome gains (orange) and losses (blue) calculated by stochastic simulations (bars, gains $4.7 \pm 4.9\%$, losses 1.8 ± 2.3 %) and mean field model (transparent area, gains 4.2%, losses 1.8%) after $t = 17$ d. Results are mean $\pm$ standard deviation if not stated otherwise. Chromosome gains and losses are normalized by number of aneuploid cells. **f**, Percentage of chromosome gains (orange bars, $4.3 \pm 3.4\%$) and losses (blue bars, $1.8 \pm 3.3\%$) experimentally measured in DN4 stage of aneuploid thymus cells (Trakala et al., 2021). **g** and **h**, Chromosome gain/loss ratio and cell fitness (color plots, values denoted along black lines) for different values of proliferation and apoptosis of monosomies. Black arrow besides the color bar denotes increasing trend. In panel **g** transition from small to high gain/loss ratio (from blue to green) is denoted

by the white arrow, experimentally measured gain/loss ratio is 2.4 (white line). Parameters corresponding to scenario S1 and S2 are depicted (white circles). In panel **h** white line represents experimentally measured gain/loss ratio from panel **g**. Parameters in panels **c**, **d**, **e**, **g**, **h** are given in **Table 1** unless stated otherwise.

Table 1. Parameters used in the model.

Parameters		Value	Source
Proliferation of diploid cells	$\beta(\mathbf{K}_{2n})$	$\ln 2\ \mathrm{d}^{-1}$	(Petrie & Zúñiga-Pflücker, 2007)
Proliferation of cells with chr. gains	$\beta(K_{+})$	$0.8 \ln 2\ \mathrm{d}^{-1}$	(Hintzen et al., 2021; Williams et al., 2008)
Proliferation of cells with chr. losses	$\beta(K_{-})$	$0.8 \ln 2\ \mathrm{d}^{-1}$	(Hintzen et al., 2021; Williams et al., 2008)
Missegregation	p_0	0.0017	Measured here
Apoptosis of diploid cells	$p_{\mathrm{a}}(\mathbf{K}_{2n})$	0	Estimated
Apoptosis of cells with chr. gain	$p_{\mathrm{a}}(K_{+})$	0	Varied here
Apoptosis of cells with chromosome loss	$p_{\mathrm{a}}(K_{-})$	0.2	Varied here

Karyotype-dependent proliferation drives the evolution of a tumor-specific karyotype with gain of chromosome 15

In contrast to pretumor karyotypes, in which there is no bias for gain of any specific chromosome, karyotypes of T-cell lymphomas are characterized by high occurrence of a chromosomes 14 and 15 (Shoshani et al., 2021; Trakala et al., 2021). As the first step in understanding the evolution of this tumor-specific karyotype, we use our model to explore a simple case where a single chromosome, referred to as chromosome 15, appears with substantially larger gain in comparison to other chromosomes, whereas in the second step we explore a more realistic case of simultaneous gains of two chromosomes. We ask under what conditions the model reproduces experimental data for gains of a specific chromosome and all other chromosomes throughout pretumor and tumor stages (**Fig. 3a**).

In a manner analogous to theory for pretumor karyotype evolution, we explore 2 scenarios: cells with gain of chromosome 15 have increased proliferation (S3) or decreased apoptosis (S4) in comparison to other aneuploid karyotypes. To test scenario S3, we varied the proliferation rate of these cells. A pedigree tree depicts how faster proliferation leads to domination of cells with gain of chromosome 15 (**Fig. 3b**). The whole evolution of this macro-karyotype over pretumor and tumor stages is obtained by solving Eq. (3) (**Fig. 3c**). For the first 2-3 days, gain of chromosome 15 and gain of other chromosomes follow a similar trend. Later in time, gain of chromosome 15 increases faster than gains of other chromosomes. Strikingly, after 20 days, 10% – 40% cells gained chromosome 15 and after 40 days this fraction reaches 60% – 98%. In contrast, gain of other chromosomes is below 10% for all time points.

These theoretical results are in agreement with experiments, which showed that gain of chromosomes 15 is around 90% whereas gain of other chromosomes is around 10% (**Fig. 3c**). This pronounced gain of specific chromosomes is a robust result of our theory because this gain

appears for different proliferations and persists afterwards. Our theory also reproduces the main features of karyotype evolution during earlier stages of T-cell development, including steady increase in chromosome gains during DN1-DN4 stages followed by a sharper increase in double positive (DP) stage (**Fig. 3c**), supporting the idea of proliferation-driven karyotype evolution.

We also tested robustness of our mean-field result by performing stochastic simulations that corresponds to a realistic situation with a finite number of cells. Indeed, stochastic simulations after 40 days showed same trends as mean-field theory, with pronounced gain of a specific chromosome and lower average gain of other chromosomes (compare **Figs. 3c** and **3d**). In experiments it was found that T-cell lymphomas were highly aneuploid and almost all cells contained gain of chromosome 15 (**Fig. 3e**). By comparing the distributions obtained by stochastic simulations and experiments, we find that they are different for chromosome losses, but not for chromosome gains (two sample Kolmogorov-Smirnov test, p-value is 0.2 for chromosome gains and 0.03 for chromosome losses). The agreement between experiments and theory suggests that increased proliferation of cells with gain of chromosome 15 is the main reason for gain of specific chromosomes in tumor karyotypes.

To test scenario S4 in which cells with gain of chromosome 15 have decreased apoptosis, we set that these cells and euploid cells do not undergo apoptosis, whereas the probability of apoptosis is 20% for other aneuploid cells. In contrast to scenario S3, which resulted in a pronounced gain of chromosome 15 (**Fig. 3c**), we find that in scenario S4 all gains stay at a low value, below 2% (**Fig. 3f**). Thus, the karyotype distribution obtained by these parameters cannot reproduce the experimentally observed high occurrence of chromosome 15 (**Fig. 3g**). In particular, although this theoretical result can explain early stages of T-cell evolution, there is a big discrepancy with experiments for later stages. Therefore, we conclude that reduced apoptosis of cells with gain of chromosome 15 cannot explain the experimentally observed karyotype evolution, additionally strengthening the idea that this process is driven by increased proliferation of these cells.

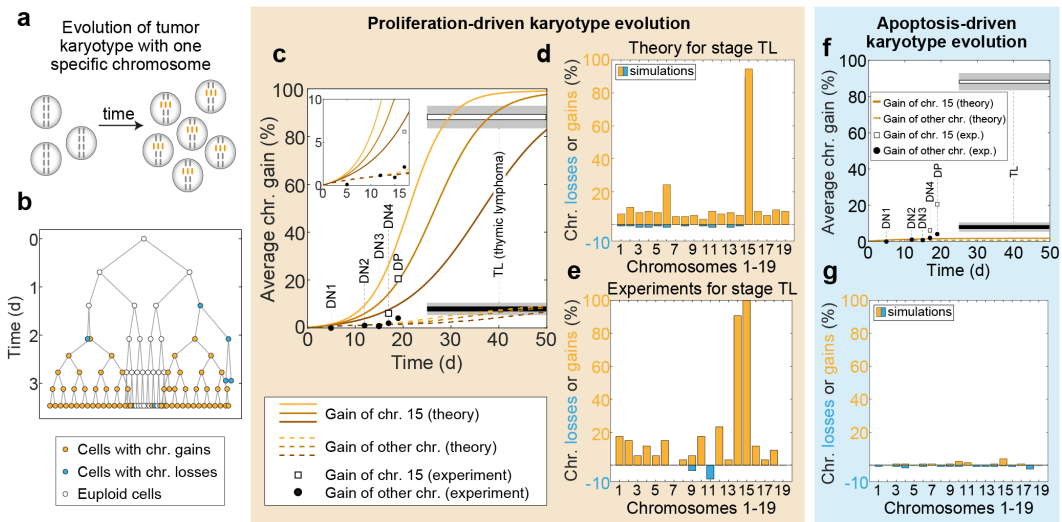

Figure 3. Increased proliferation of cells with trisomy of chromosome 15 drives the evolution of a tumor-specific karyotype. a, Schematics showing cells containing two copies of chromosomes (gray rods) and three copies of a specific chromosome (orange rods) at two different time points. **b,** Pedigree tree obtained from one simulation run, showing diploid cells (white circles), cells with gains (orange circles) and losses (blue circles). **c,** Solutions of the mean field model showing time evolution of gain of chromosome 15 (full lines) and gain of other chromosomes (dashed lines) for 3 different proliferation rates, $\beta(K_{+15}) = 1.15\ \mathrm{d}^{-1}$(dark orange lines), $\beta(K_{+15}) = 1.25\ \mathrm{d}^{-1}$(orange lines), $\beta(K_{+15}) = 1.35\ \mathrm{d}^{-1}$(light orange lines). Experimentally measured gains (black circles) in different stages of T-cell

lymphomas development. In stages DN4, DP and TL gain of chromosome 15 is depicted separately (white rectangles). Due to experimental uncertainty, values for TL stage are shown for a broad time interval, depicted as long white (chromosome 15), black (other chromosomes) and gray rectangles (standard error of mean). Insert enlarges the first 18 days of T-cell development (DN1-DN4 stages). **d,** Percentage of chromosome gains (orange bars) and losses (blue bars) calculated by stochastic simulations obtained after $t = 40$ d. Parameters same as for middle orange line in panel **c**. Gain of chromosome 15 is 94.4% and loss is 0%, whereas average gain of other chromosomes is $7.8 \pm 4.4\%$ and average loss is $0.72 \pm 0.67\%$ **e,** Percentage of chromosome gains (orange bars) and losses (blue bars) experimentally measured in T-cell lymphomas (Trakala et al., 2021). Average gain of chromosomes 14 and 15 is $95.4 \pm 6.5\%$ and average loss is 0%, whereas average gain of other chromosomes is $8.7 \pm 7.1\%$ and average loss is $0.7 \pm 2.1\%$. **f,** Solutions of the mean field model showing time evolution of gain of chromosome 15 (full line) and gain of other chromosomes (dashed line) for parameters $p_a(K_{+15}) = 0$ and $p_a(\mathbf{K} \neq \mathbf{K}_{2n}) = 0.2$. Experimental points are same as in panel **c**. **g,** Percentage of chromosome gains (orange bars) and losses (blue bars) calculated by stochastic simulations for parameters from panel **f**. Parameters in panels **b**, **c**, **d**, **f** and **g** are given in **Table 1** unless stated otherwise.

Tumor karyotypes with gains of two chromosomes arise due to karyotype-dependent proliferation alone or together with karyotype-dependent apoptosis

To explore the case of simultaneous gains of two chromosomes (**Fig. 4a**), as observed in experiments, we test the scenario where cells with simultaneous gains of both specific chromosomes, 14 and 15, have proliferative advantage compared to all other karyotypes (S5) or scenario in which these two chromosomes regulate different processes, apoptosis and proliferation (S6). In scenario S5, where the proliferation rate of cells with gains of chromosomes 14 and 15 is increased (**Fig. 4b, 4c**), we find that during the first 10 days all chromosomes follow a similar trend, whereas later in time gains of chromosomes 14 and 15 increase fast and approach 100%, while the gains of other chromosomes remain at around 10%. The general trend in **Fig. 4b** is similar to the scenario S3 based on increased proliferation for gains of a single chromosome (**Fig. 3c**), but in **Fig. 4b** we observe that gain of specific chromosomes occurs later in time in comparison to **Fig. 3c**. This time lag occurs because it is less likely to gain two specific chromosomes than only one. Interestingly, even though we required that karyotypes have gain of two specific chromosomes, which seems as a more rigid constraint than gain of only one chromosome, the agreement between experiments and theory additionally improves (compare **Figs. 3c** and **4b**). These results suggest that enhanced proliferation of cells with gain of both specific chromosomes can drive development of T-cell lymphomas.

Finally, we explore scenario S6 in which cells with gain of chromosome 14 have decreased apoptosis, whereas cells with gain of chromosome 15 have increased proliferation. Again, we find that increased proliferation leads to faster appearance of the corresponding chromosome gains than decreased apoptosis (**Fig. 4d**). Surprisingly, we find that decreased apoptosis leads to fast accumulation of cells with gain of chromosome 14, due to high proliferation of these cells given that they also have gain of chromosome 15. This is in contrast to the scenario S4, where decreased apoptosis had a minor effect on chromosome gains because of lack of proliferative advantage of any karyotype.

Taken together, our model predicts that tumor karyotypes characterized by high occurrence of one specific chromosome can be explained by proliferation-driven evolution of aneuploid cells. In the case of tumor karyotypes with two specific chromosomes, the model predicts that such karyotypes can arise by evolution that is driven by karyotype-dependent proliferation or by an interplay of proliferation and apoptosis.

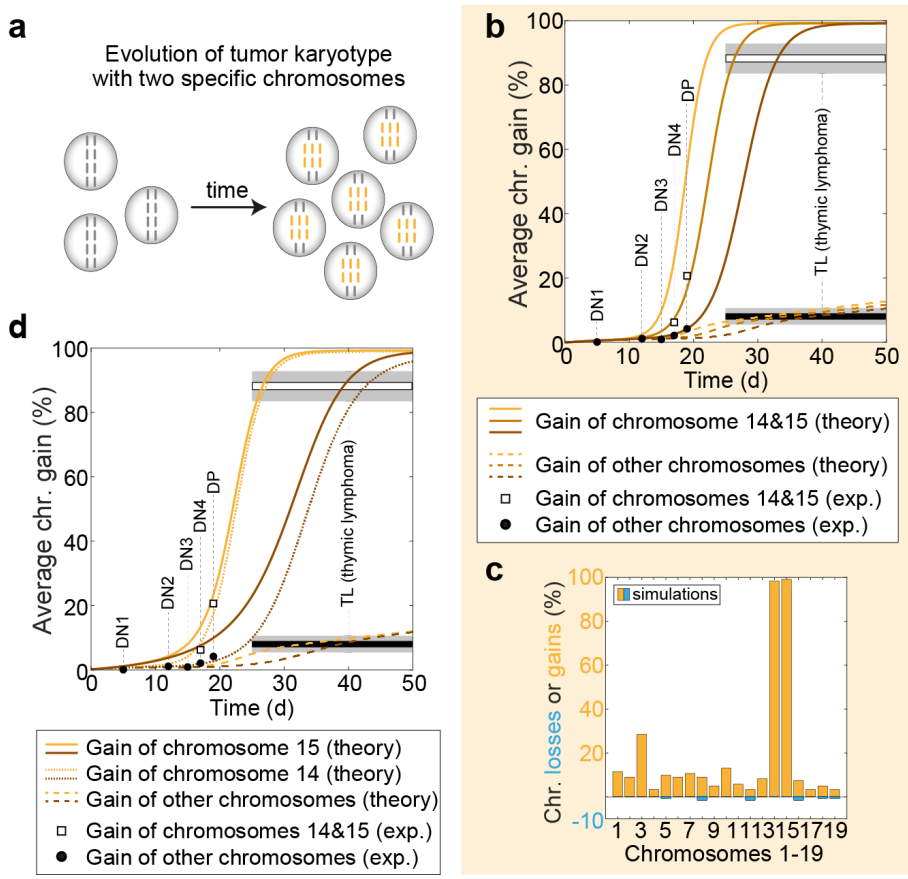

Figure 4. Tumor karyotypes with gains of chromosomes 14 and 15 arise due to karyotype-dependent proliferation alone or together with karyotype-dependent apoptosis. a, Schematics showing cells containing two copies of chromosomes (gray rods) and three copies of two specific chromosomes (orange rods) at two different time points. **b,** Solutions of the mean field model showing time evolution of gain of chromosomes 14 and 15 (full lines) and gain of other chromosome (dashed lines) for 3 different proliferation rates, $\beta(K_{+14,+15}) = 1.6\ \mathrm{d}^{-1}$(dark orange lines), $\beta(K_{+14,+15}) = 1.8\ \mathrm{d}^{-1}$(orange lines), $\beta(K_{+14,+15}) = 2.0\ \mathrm{d}^{-1}$(light orange lines). **c,** Percentage of chromosome gains (orange bars) and losses (blue bars) calculated by stochastic simulations after $t = 40$ d for parameters from panel **b** (middle lines). **d,** Solutions of the mean field model showing time evolution of gains of chromosome 14 (dotted lines), chromosome 15 (full lines) and other chromosomes (dashed lines), for 2 different probabilities of apoptosis $p(K_{+14}) = 0.02$ (orange lines) and $p(K_{+14}) = 0.2$ (dark orange lines). Apoptosis of other aneuploid karyotypes is set to $p(\mathbf{K}\neq\mathbf{K}_{2n}) = 0.2$ and proliferation rate is $\beta(K_{+15}) = 1.8\ \mathrm{d}^{-1}$. Experimental points in panels **b** and **d** are same as in **Fig 3c**. Parameters in panels **b-d** are given in **Table 1** unless stated otherwise.

DISCUSSION

In this study we developed a theoretical model by which we explored karyotype evolution in mouse model with enhanced chromosome missegregation. By quantitative comparison of our theoretical results and experimentally observed karyotypes in different stages of development of thymic lymphomas, we found that cell proliferation plays a key role in selection of a specific chromosome. It will be interesting to apply this model to patients derived human tumors (ref.

baza podataka), to explore interplay between karyotype-dependent proliferation, apoptosis, and missegregation in the evolution of these tumors.

In addition to these processes, numerous studies show that tetraploidization is an important pathway to aneuploidy in human cancer cells, which is based on direct observations of this process in tumor cell lines (Cimini et al., 1999; Shi & King, 2005) and deduced from distribution of chromosome numbers in different tumors (Storchova & Kuffer, 2008). In order to investigate theoretically the role of this pathway and its interplay with other processes, our model can be extended by including whole genome duplication as an additional choice of cell fate at each division. Whole genome duplication has been suggested as a key process leading to near triploid karyotypes often observed in tumors (Elizalde et al., 2018; Laughney et al., 2015), but it will be interesting to explore the importance of karyotype dependent proliferation in evolution of these karyotypes.

As in the mouse model with enhanced missegregation, karyotypes in different human tumors and different patients also have pronounced gains/losses of specific chromosomes (Bolhaqueiro et al., 2019; Liu et al., 2018). Our study suggests that faster proliferation of cells with specific chromosome gains drives development of human tumor karyotypes. To explore this exciting hypothesis, it will be crucial to assess experimentally how the key processes underlying tumor development depend on the cell karyotype.

REFERENCES

Araujo, A., Baum, B., & Bentley, P. (2013). The Role of Chromosome Missegregation in Cancer Development: A Theoretical Approach Using Agent-Based Modelling. *PLOS ONE*, *8*(8), e72206. https://doi.org/10.1371/JOURNAL.PONE.0072206

Bakhoum, S. F., Genovese, G., & Compton, D. A. (2009). Deviant Kinetochore Microtubule Dynamics Underlie Chromosomal Instability. *Current Biology*, *19*(22), 1937–1942. https://doi.org/10.1016/j.cub.2009.09.055

Ben-David, U., & Amon, A. (2019). Context is everything: aneuploidy in cancer. *Nature Reviews Genetics 2019 21:1*, *21*(1), 44–62. https://doi.org/10.1038/s41576-019-0171-x

Ben-David, U., Arad, G., Weissbein, U., Mandefro, B., Maimon, A., Golan-Lev, T., Narwani, K., Clark, A. T., Andrews, P. W., Benvenisty, N., & Biancotti, J. C. (2014). Aneuploidy induces profound changes in gene expression, proliferation and tumorigenicity of human pluripotent stem cells. *Nature Communications*, *5*(4825). https://doi.org/10.1038/ncomms5825

Bolhaqueiro, A. C. F., Ponsioen, B., Bakker, B., Klaasen, S. J., Kucukkose, E., van Jaarsveld, R. H., Vivié, J., Verlaan-Klink, I., Hami, N., Spierings, D. C. J., Sasaki, N., Dutta, D., Boj, S. F., Vries, R. G. J., Lansdorp, P. M., van de Wetering, M., van Oudenaarden, A., Clevers, H., Kranenburg, O., … Kops, G. J. P. L. (2019). Ongoing chromosomal instability and karyotype evolution in human colorectal cancer organoids. *Nature Genetics*, *51*(5), 824–834. https://doi.org/10.1038/s41588-019-0399-6

Bolton, H., Graham, S. J. L., van der Aa, N., Kumar, P., Theunis, K., Fernandez Gallardo, E., Voet, T., & Zernicka-Goetz, M. (2016). Mouse model of chromosome mosaicism reveals lineage-specific depletion of aneuploid cells and normal developmental potential. *Nature Communications 2016 7:1*, *7*(1), 1–12. https://doi.org/10.1038/ncomms11165

Cimini, D. (2008). Merotelic kinetochore orientation, aneuploidy, and cancer. In *Biochimica et Biophysica Acta - Reviews on Cancer* (Vol. 1786, Issue 1, pp. 32–40). https://doi.org/10.1016/j.bbcan.2008.05.003

Cimini, D., Howell, B., Maddox, P., Khodjakov, A., Degrassi, F., & Salmon, E. D. (2001). Merotelic Kinetochore Orientation Is a Major Mechanism of Aneuploidy in Mitotic Mammalian Tissue Cells 7. *The Journal of Cell Biology*, *153*(3), 517–527. http://www.jcb.org/cgi/content/full/153/3/517

Cimini, D., Tanzarella, C., & Degrassi, F. (1999). Differences in malsegregation rates obtained by scoring ana-telophases or binucleate cells. *Mutagenesis*, *14*(6), 563–568. https://doi.org/10.1093/MUTAGE/14.6.563

Desper, R., Difilippantonio, M. J., Ried, T., & Schäffer, A. A. (2005). A comprehensive continuous-time model for the appearance of CGH signal due to chromosomal missegregations during mitosis. *National Institutes of Health*, 67–87.

Dewhurst, S. M., McGranahan, N., Burrell, R. A., Rowan, A. J., Grönroos, E., Endesfelder, D., Joshi, T., Mouradov, D., Gibbs, P., Ward, R. L., Hawkins, N. J., Szallasi, Z., Sieber, O. M., & Swanton, C. (2014). Tolerance of whole- genome doubling propagates chromosomal instability and accelerates cancer genome evolution. *Cancer Discovery*, *4*(2), 175–185. https://doi.org/10.1158/2159-8290.CD-13-0285

Drost, J., & Clevers, H. (2018). Organoids in cancer research. *Nature Reviews. Cancer*, *18*(7), 407–418. https://doi.org/10.1038/S41568-018-0007-6

Duijf, P. H. G., & Benezra, R. (2013). The cancer biology of whole-chromosome instability. In *Oncogene* (Vol. 32, Issue 40, pp. 4727–4736). https://doi.org/10.1038/onc.2012.616

Elizalde, S., Laughney, A. M., & Bakhoum, S. F. (2018). A Markov chain for numerical chromosomal instability in clonally expanding populations. *PLoS Computational Biology*, *14*(9). https://doi.org/10.1371/journal.pcbi.1006447

Gordon, D. J., Resio, B., & Pellman, D. (2012). Causes and consequences of aneuploidy in cancer. *Nature Reviews Genetics 2012 13:3*, *13*(3), 189–203. https://doi.org/10.1038/nrg3123

Gusev, Y., Kagansky+, V., & Dooley, W. C. (2001). Long-Term Dynamics of Chromosomal Instability in Cancer: A Transition Probability Model. *Mathematical and Computer Modelling*, *33*, 1253–1273. www.elsevier.nl/locate/mcm

Gusev, Y., Kagansky, V., & Dooley, W. C. (2000). A Stochastic Model of Chromosome Segregation Errors with Reference to Cancer Cells. *Mathematical and Computer Modelling*, *32*, 97–111. www.el~vier.nl/locate/mcm

Heyde, A., Rohde, D., McAlpine, C. S., Zhang, S., Hoyer, F. F., Gerold, J. M., Cheek, D., Iwamoto, Y., Schloss, M. J., Vandoorne, K., Iborra-Egea, O., Muñoz-Guijosa, C., Bayes-Genis, A., Reiter, J. G., Craig, M., Swirski, F. K., Nahrendorf, M., Nowak, M. A., & Naxerova, K. (2021). Increased stem cell proliferation in atherosclerosis accelerates clonal hematopoiesis. *Cell*, *184*(5), 1348-1361.e22. https://doi.org/10.1016/J.CELL.2021.01.049

Hintzen, D. C., Soto, M., Schubert, M., Bakker, B., Spierings, D. C., Szuhai, K., Lansdorp, P. M., Foijer, F., Medema, R. H., & Raaijmakers, J. A. (2021). Monosomies, trisomies and segmental aneuploidies differentially affect chromosomal stability. *BioRxiv*. https://doi.org/10.1101/2021.08.31.458318

Hwang, S., Cavaliere, P., Li, R., Zhu, L. J., Dephoure, N., & Torres, E. M. (2021). Consequences of aneuploidy in human fibroblasts with trisomy 21. *Proceedings of the National Academy of Sciences of the United States of America*, *118*(6). https://doi.org/10.1073/PNAS.2014723118/SUPPL_FILE/PNAS.2014723118.SD05.XLSX

Laughney, A. M., Elizalde, S., Genovese, G., & Bakhoum, S. F. (2015). Dynamics of Tumor Heterogeneity Derived from Clonal Karyotypic Evolution. *Cell Reports*, *12*(5), 809–820. https://doi.org/10.1016/j.celrep.2015.06.065

Liu, Y., Sethi, N. S., Hinoue, T., Schneider, B. G., Cherniack, A. D., Sanchez-Vega, F., Seoane, J. A., Farshidfar, F., Bowlby, R., Islam, M., Kim, J., Chatila, W., Akbani, R., Kanchi, R. S., Rabkin, C. S., Willis, J. E., Wang, K. K., McCall, S. J., Mishra, L., … Laird, P. W. (2018). Comparative Molecular Analysis of Gastrointestinal Adenocarcinomas. *Cancer Cell*, *33*(4), 721-735.e8. https://doi.org/10.1016/J.CCELL.2018.03.010

Lynch, A. R., Arp, N. L., Zhou, A. S., Weaver, B. A., Burkard, M. E., & Burkard, M. (2021). Quantifying chromosomal instability from intratumoral karyotype diversity using agent-based modeling and Bayesian inference. *BioRxiv*. https://doi.org/10.1101/2021.04.26.441466

Narkar, A., Johnson, B. A., Bharne, P., Zhu, J., Padmanaban, V., Biswas, D., Fraser, A., Iglesias, P. A., Ewald, A. J., & Li, R. (2021). On the role of p53 in the cellular response to aneuploidy. *Cell Reports*, *34*(12). https://doi.org/10.1016/J.CELREP.2021.108892

Nicholson, J. M., & Cimini, D. (2013). Cancer karyotypes: Survival of the fittest. In *Frontiers in Oncology: Vol. 3 JUN*. https://doi.org/10.3389/fonc.2013.00148

Nicholson, J. M., Macedo, J. C., Mattingly, A. J., Wangsa, D., Camps, J., Lima, V., Gomes, A. M., Ried, T., Logarinho, E., & Cimini, D. (2015). Chromosome mis-segregation and cytokinesis failure in trisomic human cells. *ELIFE*, *4*(e05068). https://doi.org/10.7554/eLife.05068.001

Petrie, H. T., & Zúñiga-Pflücker, J. C. (2007). Zoned out: functional mapping of stromal signaling microenvironments in the thymus. In *Annual Review of Immunology* (Vol. 25, pp. 649–679). https://doi.org/10.1146/annurev.immunol.23.021704.115715

Porritt, H. E., Gordon, K., & Petrie, H. T. (2003). Kinetics of steady-state differentiation and mapping of intrathymic-signaling environments by stem cell transplantation in nonirradiated mice. *Journal of Experimental Medicine*, *198*(6), 957–962. https://doi.org/10.1084/jem.20030837

Rohban, S., & Campaner, S. (2015). Myc induced replicative stress response: How to cope with it and exploit it. In *Biochimica et Biophysica Acta - Gene Regulatory Mechanisms* (Vol. 1849, Issue 5, pp. 517–524). Elsevier B.V. https://doi.org/10.1016/j.bbagrm.2014.04.008

Santaguida, S., Vasile, E., White, E., & Amon, A. (2015). Aneuploidy-induced cellular stresses limit autophagic degradation. *Genes and Development*, *29*(19), 2010–2021. https://doi.org/10.1101/gad.269118.115

Sheppard, O., Wiseman, F. K., Ruparelia, A., Tybulewicz, V. L. J., & Fisher, E. M. C. (2012). Mouse Models of Aneuploidy. *The Scientific World Journal*, *2012*. https://doi.org/10.1100/2012/214078

Shi, Q., & King, R. W. (2005). Chromosome nondisjunction yields tetraploid rather than aneuploid cells in human cell lines. *Nature*, *437*(7061), 1038–1042. https://doi.org/10.1038/nature03958

Shoshani, O., Bakker, B., de Haan, L., Tijhuis, A. E., Wang, Y., Kim, D. H., Maldonado, M., Demarest, M. A., Artates, J., Zhengyu, O., Mark, A., Wardenaar, R., Sasik, R., Spierings, D. C. J., Vitre, B., Fisch, K., Foijer, F., & Cleveland, D. W. (2021). Transient genomic instability drives tumorigenesis through accelerated clonal evolution. *Genes & Development*, *35*(15–16), 1093–1109. https://doi.org/10.1101/GAD.348319.121

Storchova, Z., & Kuffer, C. (2008). The consequences of tetraploidy and aneuploidy. In *Journal of Cell Science* (Vol. 121, Issue 23, pp. 3859–3866). https://doi.org/10.1242/jcs.039537

Thompson, S. L., & Compton, D. A. (2008). Examining the link between chromosomal instability and aneuploidy in human cells. *Journal of Cell Biology*, *180*(4), 665–672. https://doi.org/10.1083/jcb.200712029

Thompson, S. L., & Compton, D. A. (2011a). Chromosome missegregation in human cells arises through specific types of kinetochore-microtubule attachment errors. *PNAS*, *108*(44), 17974–17978. https://doi.org/10.1073/pnas.1109720108

Thompson, S. L., & Compton, D. A. (2011b). Chromosome missegregation in human cells arises through specific types of kinetochore-microtubule attachment errors. *Proceedings of the National Academy of Sciences of the United States of America*, *108*(44), 17974–17978. https://doi.org/10.1073/pnas.1109720108

Trakala, M., Aggarwal, M., Sniffen, C., Zasadil, L., Carroll, A., Ma, D., Su, X. A., Wangsa, D., Meyer, A., Sieben, C. J., Zhong, J., Hsu, P. H., Paradis, G., Ried, T., Holland, A., van Deursen, J., & Amon, A. (2021). Clonal selection of stable aneuploidies in progenitor cells drives high-prevalence tumorigenesis. *Genes and Development*, *35*(15–16), 1079–1092. https://doi.org/10.1101/gad.348341.121

van Jaarsveld, R. H., & Kops, G. J. P. L. (2016). Difference Makers: Chromosomal Instability versus Aneuploidy in Cancer. *Trends in Cancer*, *2*(10), 561–571. https://doi.org/10.1016/J.TRECAN.2016.09.003

Weaver, B. A., & Cleveland, D. W. (2006). Does aneuploidy cause cancer? *Current Opinion in Cell Biology*, *18*(6), 658–667. https://doi.org/10.1016/J.CEB.2006.10.002

Williams, B. R., Prabhu, V. R., Hunter, K. E., Glazier, C. M., Whittaker, C. A., Housman, D. E., & Amon, A. (2008). Aneuploidy Affects Proliferation and Spontaneous Immortalization in Mammalian Cells Downloaded from. *Science*, *322*, 703–708. www.sciencemag.orgSCIENCEVOLhttp://science.sciencemag.org/